Determination of the Partial Structure Factors of the Metallic Glass $Fe_{80}B_{20}$

E. Nold, P. Lamparter, H. Olbrich, G. Rainer-Harbach, and S. Steeb
Max-Planck-Institut für Metallforschung, Institut für Werkstoffwissenschaften, Stuttgart

Z. Naturforsch. **36a**, 1032–1044 (1981); received August 2, 1981

By X-ray diffraction and neutron diffraction using the isotopic substitution method, the partial structure factors S_{FeFe}, S_{FeB}, and S_{BB} as well as S_{NN}, S_{CC}, and S_{NC} were determined for the metallic glass $Fe_{80}B_{20}$. The Fourier-transforms yielded the pair correlation functions G_{ij} from which the atomic distances and the partial coordination numbers were calculated. The partial coordination numbers are in good agreement with those of the metastable Fe_3B-phase, which is the first crystallization product formed during annealing of the metallic glass $Fe_{80}B_{20}$. The chemical short range order parameter amounts to 100%, thus indicating perfect chemical order.

Introduction

It is the aim of the present paper to investigate by means of diffraction experiments the mutual distribution of the components in the metallic glass $Fe_{80}B_{20}$. For this purpose three independent diffraction experiments have to be performed, in each of which the ratio of the scattering powers of Fe and B must be different. This can be achieved either by applying different radiations or by using isotopes with different scattering lengths in preparing samples with the same chemical composition for neutron scattering experiments. In the present work both methods have been combined.

Theoretical Fundamentals

We will only present a short compilation of the equations needed for the evaluation of the three partial structure factors. For a comprehensive presentation see Refs. [1] to [4]. The scattering behaviour of an isotropic binary molten or amorphous alloy can be described by three partial structure factors $S_{ij}(Q)$, where $S_{ij}(Q) = S_{ji}(Q)$. From these partial functions the total function can be obtained

$$\begin{aligned} S(Q) &= \frac{c_A^2 b_A^2}{\langle b\rangle^2} S_{AA}(Q) + \frac{c_B^2 b_B^2}{\langle b\rangle^2} S_{BB}(Q) \\ &\quad + \frac{2 c_A c_B b_A b_B}{\langle b\rangle^2} S_{AB}(Q) \\ &= W_{AA} S_{AA}(Q) + W_{BB} S_{BB}(Q) \\ &\quad + W_{AB} S_{AB}(Q) \end{aligned} \tag{1}$$

Reprint requests to Prof. S. Steeb, Max-Planck-Institut für Metallforschung, Inst. f. Werkstoffwissenschaften, Seestraße 92, D-7000 Stuttgart 1.

with c_i concentration of component i in atomic fractions, b_i scattering length of the atoms of component i, $\langle b\rangle = c_A b_A + c_B b_B$.

The total structure factor $S(Q)$ is obtained from the coherently scattered intensity per atom $I_n(Q)$ which follows from the measured intensity by a correction- and normalization-procedure. The following equation stands according to the Faber-Ziman definition [5]:

$$S(Q) = \frac{I_n(Q) - \mathrm{LMS}}{\langle b\rangle^2}. \tag{2}$$

The Laue monotonic scattering LMS

$$\mathrm{LMS} = \langle b^2\rangle - \langle b\rangle^2 = c_A c_B (\Delta b)^2 \tag{3}$$

is regarded as part of the coherent scattering and is subtracted in (2). The LMS is observed in the unmodulated form given by (3) if the atoms of both components with their different scattering lengths are distributed statistically within the global structure (see for example [6]).

According to Ashcroft and Langreth [7] a total structure factor for a binary system can also be defined in the following way:

$$S^{AL}(Q) = I_n(Q)/\langle b^2\rangle. \tag{4}$$

By this procedure the LMS is not subtracted and there is a normalization to $\langle b^2\rangle$ and not to $\langle b\rangle^2$ as in (3).

In neutron diffraction experiments with materials containing atoms M with a magnetic moment an additional scattering contribution $I_m(Q)$ will occur which has its origin in the interaction of the magnetic moments of neutrons and the atoms M:

$$I_m(Q) = P^2(Q)\, S_{MM}(Q) \sin^2\alpha \tag{5}$$

0340-4811 / 81 / 1000-1032 $ 01.00/0. – Please order a reprint rather than making your own copy.

with $P(Q)$ magnetic scattering length, $S_{MM}(Q)$ partial structure factor of the M-M-atomic pairs, α angle between atomic magnetic moment and scattering vector $\boldsymbol{Q}$.

The magnetic moment of the iron atoms causes the Q-dependent scattering length $P(Q)$ in addition to the Q-independent scattering length of the nucleus [8]:

$$P(Q) = \frac{r_0 \gamma}{2} |\boldsymbol{\mu}| F(Q). \tag{6}$$

r_0 means the classical electron radius ($2.8 \cdot 10^{-13}$ cm), γ the magnetic moment of the neutron (-1.91), and $|\boldsymbol{\mu}|$ the total of the atomic magnetic moment. $F(Q)$ means the magnetic form factor, which is normalized to one for $Q=0$ and which decreases to zero with increasing Q. The magnetic scattering contribution becomes zero according to (5) if the atomic magnetic moments are aligned by means of an external magnetic field parallel to $\boldsymbol{Q}$.

From the total structure factor $S(Q)$ in (1) by Fourier transformation according to (7) the total pair distribution function $g(r)$ and the total reduced pair distribution function $G(r)$ are obtained:

$$\begin{aligned} G(r) &= 4\pi r \varrho_0 [g(r) - 1] \\ &= \frac{2}{\pi} \int_0^\infty Q[S(Q) - 1] \sin(Qr)\, dQ. \end{aligned} \tag{7}$$

The total pair distribution function $g(r)$ is a weighted sum of the three partial pair distribution functions according to (8):

$$\begin{aligned} g(r) &= \frac{c_A^2 b_A^2}{\langle b \rangle^2} g_{AA}(r) + \frac{c_B^2 b_B^2}{\langle b \rangle^2} g_{BB}(r) \\ &\quad + \frac{2 c_A c_B b_A b_B}{\langle b \rangle^2} g_{AB}(r) \\ &= W_{AA} g_{AA}(r) + W_{BB} g_{BB}(r) \\ &\quad + W_{AB} g_{AB}(r). \end{aligned} \tag{8}$$

The total radial distribution function RDF(r) is obtained according to (9):

$$\begin{aligned} \mathrm{RDF}(r) &= 4\pi r^2 \varrho_0 g(r) = 4\pi r^2 \varrho(r) \\ &= 4\pi r^2 \varrho_0 + r G(r) \end{aligned} \tag{9}$$

with $\varrho(r) = \varrho_0 g(r) =$ local number density and $\varrho_0 =$ mean atomic number per volume.

The partial functions can be defined as follows:

$$\begin{aligned} G_{ij}(r) &= 4\pi r \varrho_0 [g_{ij}(r) - 1] \\ &= \frac{2}{\pi} \int_0^\infty Q[S_{ij}(Q) - 1] \sin(Qr)\, dQ, \end{aligned} \tag{10}$$

$$\begin{aligned} A_{ij}(r) &= c_j 4\pi r^2 \varrho_0 g_{ij}(r) = 4\pi r^2 \varrho_{ij}(r) \\ &= c_j [4\pi r^2 \varrho_0 + r G_{ij}(r)] \end{aligned} \tag{11}$$

with $\varrho_{ij}(r) = c_j \varrho_0 g_{ij}(r) =$ partial local number density = number of j-atoms per volume element within a coordination sphere with radius r around an i-atom.

Three experiments with different weighting factors W_{ij} yield three different total structure factors which can be used to calculate the partial structure factors in (1). Using the method of neutron diffraction, different W_{ij} can be achieved by the isotopic substitution method. The coherent scattering lengths should be changed from experiment to experiment at least with one component, whereas the concentration is kept constant. During the performance of X-ray- or magnetic neutron-diffraction experiments, where we have to deal with Q-dependent scattering lengths b, also the weighting factors W_{ij} in (1) become Q-dependent.

Three scattering experiments lead to a system of three equations (1) with $S^1_{tot}(Q)$, $S^2_{tot}(Q)$, and $S^3_{tot}(Q)$ on the left hand side. The upper index means the number of the experiment. The following matrix system is appropriate to the solution of the system of linear equations:

$$[T(Q)] = [W(Q)][R(Q)] \tag{12}$$

with

$$[T(Q)] = \begin{bmatrix} S^1_{tot}(Q) \\ S^2_{tot}(Q) \\ S^3_{tot}(Q) \end{bmatrix}, \quad [R(Q)] = \begin{bmatrix} S_{AA}(Q) \\ S_{BB}(Q) \\ S_{AB}(Q) \end{bmatrix}$$

and

$$[W(Q)] = \begin{bmatrix} W^1_{AA}(Q) & W^1_{BB}(Q) & W^1_{AB}(Q) \\ W^2_{AA}(Q) & W^2_{BB}(Q) & W^2_{AB}(Q) \\ W^3_{AA}(Q) & W^3_{BB}(Q) & W^3_{AB}(Q) \end{bmatrix}. \tag{13}$$

Thus we obtain the following solution of (12):

$$\begin{aligned} [R(Q)] &= [W(Q)]^{-1} [T(Q)] \\ &= [V(Q)][T(Q)]. \end{aligned} \tag{14}$$

(14) is only soluble if the coefficient determinant is unequal to zero, i.e. if the three equations are linearly independent.

From the total radial distribution function RDF(r) from (9) the total coordination number N^{I} in the first coordination sphere is calculated as follows:

$$N^{\mathrm{I}} = \int_{r_1^{\mathrm{I}}}^{r_u^{\mathrm{I}}} \mathrm{RDF}(r)\, dr. \tag{15}$$

The lower and upper integration limits are somewhat arbitrary and depend on the respective method. The total coordination number is a weighted sum of the coordination numbers Z_{ij}, which are independent from the scattering lengths [9]:

$$N^{\mathrm{I}} = \frac{W_{\mathrm{AA}}}{c_{\mathrm{A}}} \cdot Z_{\mathrm{AA}} + \frac{W_{\mathrm{BB}}}{c_{\mathrm{B}}} \cdot Z_{\mathrm{BB}} + \frac{W_{\mathrm{AB}}}{c_{\mathrm{B}}} \cdot Z_{\mathrm{AB}}$$
$$= W'_{\mathrm{AA}} Z_{\mathrm{AA}} + W'_{\mathrm{BB}} Z_{\mathrm{BB}} + W'_{\mathrm{AB}} Z_{\mathrm{AB}}, \qquad (16)$$

where the partial coordination numbers Z_{ij} are calculated from the partial $A_{ij}(r)$ corresponding to (15). Of course, in all four integrals the integration limits must be the same. From the position of the $G_{ij}(r)$-maximum the preferred distances of the i-j-pairs are obtained.

According to Bhatia and Thornton [10] the normalized intensity $I_{\mathrm{n}}(Q)$ can be connected with correlations of density- and concentration fluctuations:

$$S^{\mathrm{BT}} = S^{\mathrm{AL}}(Q) = \frac{I_{\mathrm{n}}(Q)}{\langle b^2 \rangle} = \frac{\langle b \rangle^2}{\langle b^2 \rangle} S_{\mathrm{NN}}(Q)$$
$$+ \frac{c_{\mathrm{A}} c_{\mathrm{B}} (\Delta b)^2}{\langle b^2 \rangle} S'_{\mathrm{CC}}(Q) + \frac{2 \langle b \rangle \Delta b}{\langle b^2 \rangle} S_{\mathrm{NC}}(Q)$$
$$= W_{\mathrm{NN}}(Q) S_{\mathrm{NN}}(Q) + W_{\mathrm{CC}}(Q) S'_{\mathrm{CC}}(Q)$$
$$+ W_{\mathrm{NC}}(Q) S_{\mathrm{NC}}(Q). \qquad (17)$$

$S_{\mathrm{NN}}(Q)$ is the structure factor of the correlations of atomic number density fluctuations, $S'_{\mathrm{CC}}(Q)$ that of the correlations of concentration fluctuations, whereas $S_{\mathrm{NC}}(Q)$ contains the cross correlations between concentration fluctuations and number density fluctuations.

S_{NN} and S'_{CC} oscillate around 1, S_{NC} around 0.

The partial density- and concentration-fluctuation correlation functions $G_{\mathrm{NN}}(r)$, $G_{\mathrm{CC}}(r)$, and $G_{\mathrm{NC}}(r)$ are obtained by Fourier transformation of the partial Bhatia Thornton structure factors. They are connected to the functions $G_{ij}(r)$ of (10) in a linear way. Especially for the partial densities the following equations are valid:

$$\varrho_{\mathrm{NN}}(r) = c_{\mathrm{A}} \varrho_{\mathrm{A}}(r) + c_{\mathrm{B}} \varrho_{\mathrm{B}}(r), \qquad (18)$$

$$\varrho_{\mathrm{CC}}(r) = c_{\mathrm{B}} \varrho_{\mathrm{A}}(r) + c_{\mathrm{A}} \varrho_{\mathrm{B}}(r) - \frac{\varrho_{\mathrm{AB}}(r)}{c_{\mathrm{B}}}, \qquad (19)$$

$$\varrho_{\mathrm{NC}}(r) = c_{\mathrm{A}} c_{\mathrm{B}} (\varrho_{\mathrm{A}}(r) - \varrho_{\mathrm{B}}(r)) \qquad (20)$$

with

$$\varrho_i(r) = \varrho_{i\mathrm{A}}(r) + \varrho_{i\mathrm{B}}(r).$$

Experiments

Two specimens with the same concentration were prepared: $^{\mathrm{nat}}Fe_{80}{}^{11}B_{20}$ and $^{57}Fe_{80}{}^{11}B_{20}$. Starting materials were iron with natural isotopic abundance (99.96%; Vacuumschmelze, Hanau), a mixture of iron isotopes enriched with ^{57}Fe (99.9%; ^{57}Fe content 80.15%; Rohstoff-Einfuhr, Düsseldorf) as well as a mixture of Boron isotopes enriched with ^{11}B (97.2%; ^{11}B content 99.2%; Rohstoff-Einfuhr, Düsseldorf). The ^{11}B-powder was alloyed with the iron in ultrapure Al_2O_3-tubes (diameter 6 mm) which were closed by cemented stoppers made from Al_2O_3. The melting and annealing procedure was done at 1350 °C for three hours. Preliminary experiments had shown that by this procedure complete alloying between iron and boron occurs. The amorphous ribbons were produced from the alloys within a melt spin apparature [11]. The cuvette consisted of quartz with an orifice of 0.6 mm. The ribbons were 0.03 mm thick and had a breadth of 1.5 mm.

The specimens for the neutron diffraction experiments were prepared by joining together parallel ribbons of a length of 35 mm ($17 \times 35 \times 2.5$ mm^3). The irradiated surface was limited by a Cd-frame. The parallel arrangement of the ribbons was necessary, since during the measurement they had to be saturized magnetically. The direction of the easiest magnetization coincides with the direction of the ribbon. For the X-ray diffraction a mono ribbon layer was prepared.

The neutron diffraction experiments were done at the two axis instrument D4 [12] at the high flux reactor of the ILL, Grenoble, using a wavelength of 0.0695 nm. Since the magnetic, Q-dependent scattering contribution had to be eliminated, a permanent magnet with 0.5 T was fixed in the center of the diffractometer in such a way that the magnetic field $\boldsymbol{H}$ was always parallel to the scattering vector $\boldsymbol{Q}$. Using this arrangement one could measure only up to $Q = 84$ nm^{-1}. For $\boldsymbol{H}$ vertical to $\boldsymbol{Q}$, however, one could measure up to 170 nm^{-1}. All measurements were performed in a θ-2θ-arrangement.

The X-ray experiments with Mo-Kα-radiation were performed in transmission using a 12 kW-rotating anode generator with a graphite monochromator in the primary beam. In θ-2θ-arrangement the Q-region of the experiment was between 3 and 122 nm^{-1}. The specimen was kept in vacuum.

The corrections and the normalization procedures were performed for the X-ray- and the neutron diffraction experiment according to Refs. [13, 14]. The density ϱ_0 of $Fe_{80}B_{20}$ was taken as 95 nm^{-3} [15]. The absorption factors of the samples were measured directly by a transmission experiment. The used scattering parameters are listed in Table 1. In the following, only the special features characteristic for the present paper shall be mentioned.

Figure 1 shows the difference curve $(I_{H\perp Q} - I_{H\parallel Q})$ which represents according to (5) the magnetic scattering contribution of the iron atoms contained in the amorphous alloy $Fe_{80}B_{20}$. The difference intensity curve was subtracted from the intensity curve obtained in the $\boldsymbol{H} \perp \boldsymbol{Q}$-arrangement after correction for absorption. The curve thus obtained is caused by nuclear scattering only.

The normalization of the X-ray experiment was done according to [14], however, an absorption correction was applied (case of transmission).

Table 1. Scattering lengths and incoherent cross sections for neutrons.

	b_{coh} [10^{-12} cm]		σ_{inc} [10^{-24} cm^2]	
^{11}B	0.6	[8]	0.6*	
^{nat}Fe	0.95	[8]	0.46	[8]
^{57}Fe	0.412	[16]	2.84	[16]

* This value for Boron enriched with ^{11}B was taken a little smaller than 0.74 for Boron with natural isotopic abundance.

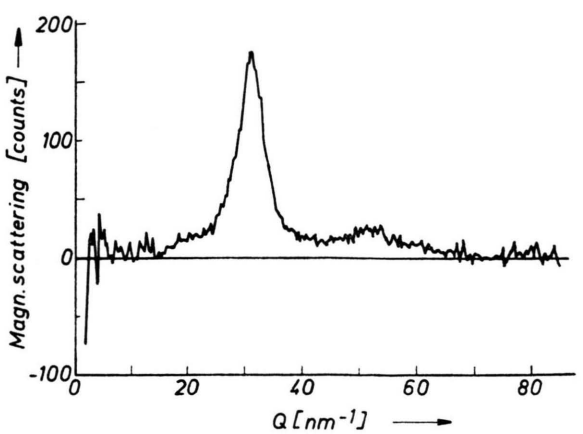

Fig. 1. Amorphous $^{57}Fe_{80}{}^{11}B_{20}$: Difference curve $I_{H\perp Q} - I_{H\parallel Q}$.

Results and Discussion

i) *Total Functions*

Figure 2 shows the total structure factors defined according to (2), which are arranged from top to bottom with decreasing ratio (b_{Fe}/b_B) of scattering lengths. The curves 2a and 2b show the behaviour as "usual" for amorphous $T_{80}M_{20}$-specimens (T = transition metals Fe, Co, Ni; M = metalloids B, C, P, Si). Table 2 contains some characteristic data of the total structure factors. The X-ray structure factor becomes negative for $Q < 25$ nm^{-1}. This behaviour is caused by the subtraction of the LMS in (2), which becomes rather large because the difference of the scattering lengths is large for X-rays:

$$\text{LMS} = c_{Fe}\, c_B\, (b_{Fe} - b_B)^2 = 0.1492\,\text{eu}\,. \qquad (3)$$

From the negative part of the structure factor one can already conclude that the presumption of statistical distribution of the atoms of both components is not valid for the specimens investigated. The total structure factor $S(Q = 10\ nm^{-1})$ amounts to -0.138, which corresponds to approximately 90% of the complete LMS-term. This means that

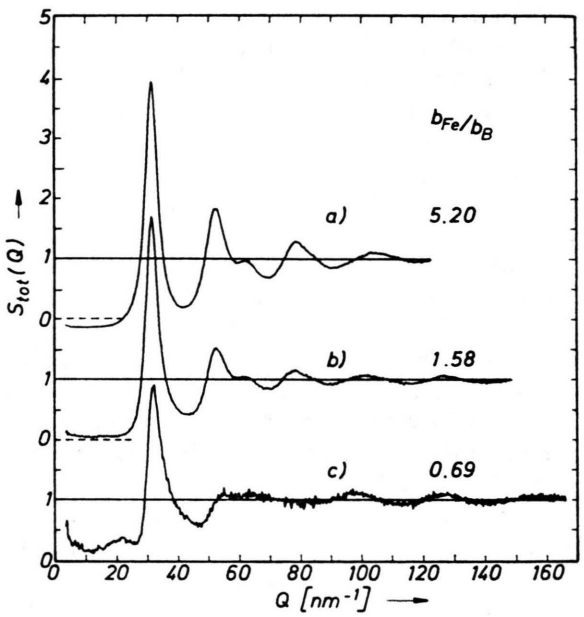

Fig. 2. Total structure factors $S_{tot}(Q)$.
a) $S^{X}_{tot}(Q)$ measured by X-rays;
b) $S^{nat}_{tot}(Q)$ measured by neutrons with $^{nat}Fe_{80}{}^{11}B_{20}$;
c) $S^{57}_{tot}(Q)$ measured by neutrons with $^{57}Fe_{80}{}^{11}B_{20}$.

Table 2. Values taken from the total functions. Q^{I}[nm^{-1}], $S(Q^{I})$: Position and height of the main maximum of $S(Q)$. $r_{ij}^{n,m}$[nm]: Distance of a j-atom within the m-th submaximum of the n-th coordination sphere of an i-atom. Some of the radii are only slightly visible as a shoulder. $N_{exp}^{n,m}$: Total coordination number determined from the m-th submaximum of the n-th coordination sphere. The integration always was done from the $r_l^{n,m}$ lower to the $r_u^{m,n}$ upper minimum. $N_c^{n,m}$: Total coordination numbers calculated from the partial coordination numbers $Z_{ij}^{n,m}$ (Table 8).

	Q^{I} $S(Q^{I})$	$r_{FeB}^{I,1}$	$r_{FeFe}^{I,2}$	$r_{FeB}^{II,1}$	$r_{FeFe}^{II,2}$	$r_{FeB}^{II,3}$	$r_{FeFe}^{II,4}$	$N_{exp}^{I,1}$ $N_c^{I,1}$ $r_l^{I,1}$ $r_u^{I,1}$	$N_{exp}^{I,2}$ $N_c^{I,2}$ $r_l^{I,2}$ $r_u^{I,2}$	$N_{exp}^{II,1}$ $N_c^{II,1}$ $r_l^{II,1}$ $r_u^{II,1}$	$N_{exp}^{II,2}$ $N_c^{II,2}$ $r_l^{II,2}$ $r_u^{II,2}$	N_{exp}^{III} N_c^{III} r_l^{III} r_u^{III}
$Fe_{80}B_{20}$(X)	31.2								14.7	21.9	30.4	73
	3.9		0.257		0.416		0.498		15.1	20.6*	28*	66*
									0.215	0.345	0.460	0.560
									0.340	0.455	0.555	0.705
$^{nat}Fe_{80}{}^{11}B_{20}$(n)	31.3								14.2	20.1	31.4	75
	3.7		0.258		0.417		0.495		14.0	—	—	—
									0.190	0.355	0.450	0.555
									0.330	0.445	0.550	0.705
$^{57}Fe_{80}{}^{11}B_{20}$(n)	31.7							4.42	7.69	17.6	26.8	70
	2.9	0.213	0.255	≃ 0.37	0.410	0.44	0.51	4.23	8.31	—	—	—
								0.190	0.240	0.315	0.43	0.52
								0.235	0.310	0.425	0.52	0.680

* Only calculated from the partial $z_{FeFe}^{n,m}$, since the integration limits of $Z_{FeB}^{n,m}$ were too different.

in fact only a small part of this scattering contribution occurs in the intensity pattern. Curve 2c, where the weighting factor W_{FeB} is comparable to W_{FeFe}, shows an uncommon behaviour in the region between the second and third maximum. Apparently a $S_{FeB}(Q)$-antiphase contribution plays a role in addition to the $S_{FeFe}(Q)$. A further feature is given by the additional maximum at $Q \cong 21.5\ nm^{-1}$, which must be assigned to the $S_{BB}(Q)$-contribution since it is not visible in the other curves. A similar maximum also occurs in the structure factor of $^{nat}Co_{81.5}{}^{11}B_{18.5}$ measured by neutron diffraction, where $b_{Co}/b_B = 0.46$ (see Ref. [17]). The total reduced pair distribution functions $G(r)$ obtained according to (7) are given in Figure 3. The total $G(r)$-functions are composed of the partial $G_{ij}(r)$-functions with the same weighting-factors $W_{ij}(Q)$ as the total structure factors (see (1) and (8)). During the Fourier-transform of the X-ray structure factor the so called Warren-Krutter-Morningstar-approach was applied [3], [4], by which the Q-dependence of the W_{ij}-weighting factors is neglected.

Figure 3a shows the Fourier-transform $G(r)$ of the X-ray structure factor, which is nearly equal to the partial $G_{FeFe}(r)$ as can be seen from the weighting factors in Table 3. In Fig. 3b an additional shoulder on the left hand side of the main maximum occurs and the minimum between the two submaxima of the second maximum has vanished. These additional features can be ascribed according to Table 3 to the partial $G_{FeB}(r)$. The Fourier-transform of the ^{57}Fe-experiment (Fig. 3c) shows a splitting up of the main maximum. The left subpeak corresponds to a B-Fe-distance and the right

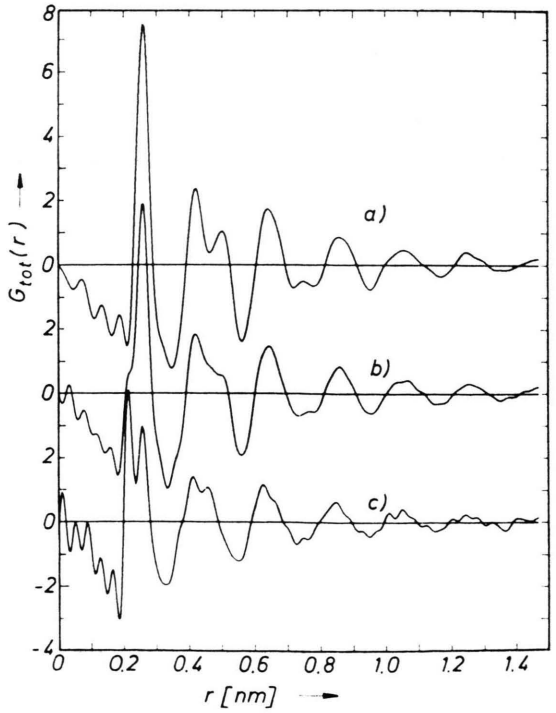

Fig. 3. Total reduced pair distribution function $G(r)$. a) $G_{tot}^{X}(Q)$; b) $G_{tot}^{nat}(Q)$; c) $G_{tot}^{57}(Q)$.

		$S^1_{tot}(Q)$ $Fe_{80}B_{20}(X)$ $Q = 0\ nm^{-1}$	$S^1_{tot}(Q)$ $Fe_{80}B_{20}(X)$ $Q = 44\ nm^{-1}$	$S^2_{tot}(Q)$ $^{nat}Fe_{80}{}^{11}B_{20}(n)$	$S^3_{tot}(Q)$ $^{57}Fe_{80}{}^{11}B_{20}(n)$
I	W_{FeFe}	0.9104	0.9446	0.7459	0.5374
	W_{BB}	0.0021	0.0008	0.0186	0.0713
	W_{FeB}	0.0875	0.0564	0.2355	0.3913
II	W'_{FeFe}	1.14		0.93	0.67
	W'_{BB}	0.01		0.09	0.36
	W'_{BFe}	0.11		0.29	0.49
	W'_{FeB}	0.44		1.18	1.96

Table 3. I) Weighting factors of the partial FZ-Structure factors in (1). For X-rays the W_{ij} are Q-dependent. II) Weighting factors of the partial coordination numbers according to (16); $(W'_{ij} = W_{ij}/c_j)$.

		$W_{NN}(Q)$	$W_{CC}(Q)$	$W_{NC}(Q)$
	$Q = 0\ nm^{-1}$	0.871	0.129	1.678
$S^1_{tot}(Q)$: $Fe_{80}B_{20}(X)$	$Q = 44\ nm^{-1}$	0.844	0.156	1.814
$S^2_{tot}(Q)$: $^{nat}Fe_{80}{}^{11}B_{20}(n)$		0.975	0.025	0.776
$S^3_{tot}(Q)$: $^{57}Fe_{80}{}^{11}B_{20}(n)$		0.973	0.027	− 0.814

Table 4. Weighting factors of the partial BT-Structure factors in (17). For X-ray the W_{ij} are Q-dependent.

subpeak to a Fe-Fe-distance. The following maxima are composed of many subpeaks, which exactly can only be identified with knowledge of the partial functions. A preliminary assignment of the single maxima or shoulders to the different Fe-Fe- and Fe-B-distances is presented in Table 2. This assignment is based on the variation of the curves with decreasing ratio of scattering lengths in connection with Table 3. The total coordination numbers are composed of the partial coordination numbers according to (16) and Table 3 (see Ref. [17]).

ii) *Partial Functions* $S_{ij}(Q)$

For the calculation of the partial structure factors a system of linear equations with the three unknowns functions of (14) must be solved. A measure concerning the efficiency of the system of equations is given by the total of a normalized determinant $W(Q)_{norm}$ which can as a maximum value achieve unity:

$$|W(Q)|_{norm} = |W_{ij}(Q)/(\Sigma_j W^2_{ij}(Q))^{1/2}|. \quad (21)$$

Since the X-ray weighting factors in (1) and (17) are Q-dependent (Tables 3 and 4), all parameters calculated from these factors are also Q-dependent. This fact had to be regarded during the calculation of the partial structure factors. The normalized determinant for $Q=0$ amounted in the FZ-formalism to 0.012 and in the BT-formalism to 0.06. For comparison it should be mentioned that during the calculation of the partial structure factors of molten RbCl the normalized determinant was 0.029 according to [18].

Table 5 contains the extrema of the determinants $[V(Q)]$ according to (14) in the FZ-formalism, Table 6 those of the BT-formalism. The figures in Tables 5 and 6 mean the multiplication factors with which the corresponding total structure factors have to be multiplied in order to obtain the

Table 5. Weighting factors of the total structure factors according to $[R(Q)]=[V(Q)][T(Q)]$ in the FZ-formalism with $[R(Q)]=[S_{FeFe}(Q), S_{BB}(Q), S_{FeB}(Q)]$ and $[T(Q)]=[S^X_{tot}(Q), S^{nat}_{tot}(Q), S^{57}_{tot}(Q)]$. The table contains the two extreme values.

$$[V^{FZ}(Q = 0\ nm^{-1})] = \begin{bmatrix} 1.8196 & -1.0364 & 0.2168 \\ 31.65 & -59.21 & 28.56 \\ -8.261 & 12.202 & -2.941 \end{bmatrix}$$

$$[V^{FZ}(Q = 44\ nm^{-1})] = \begin{bmatrix} 1.4078 & -0.5307 & 0.1229 \\ 24.49 & -50.42 & 26.93 \\ -6.391 & 9.906 & -2.515 \end{bmatrix}$$

Table 6. Weighting factors of the total structure factors according to $[R(Q)]=[V(Q)][T(Q)]$ in the BT-formalism with $[R(Q)]=[S_{NN}(Q), S_{CC}(Q), S_{NC}(Q)]$ and $[T(Q)]=[S^X_{tot}(Q), S^{nat}_{tot}(Q), S^{57}_{tot}(Q)]$. The table contains the two extreme values.

$$[V^{BT}(Q = 0\ nm^{-1})] = \begin{bmatrix} -0.2445 & 0.8950 & 0.3494 \\ 9.187 & -13.887 & 5.700 \\ 0.015 & 0.606 & -0.6207 \end{bmatrix}$$

$$[V^{BT}(Q = 44\ nm^{-1})] = \begin{bmatrix} -0.1951 & 0.8344 & 0.3607 \\ 7.332 & -11.608 & 5.276 \\ 0.012 & 0.6094 & -0.6214 \end{bmatrix}$$

partial structure factors. Especially for the case of the partial S_{BB} one can see in Table 5 that due to the multiplication factor of up to 60 a small error in the total measured functions (3% can be taken as typical) yields large uncertainties.

Therefore, the partial structure factor $S_{BB}^{exp}(Q)$, which was calculated from (14) without additional presumptions, had to be refined in order to yield a partial $S_{BB}^{fit}(Q)$ which was compatible with the experiments as well as with theory [19, 20]. This finally led to the following procedure:

The additional peak at $Q \cong 21.5\,nm^{-1}$ in the $^{57}Fe_{80}{}^{11}B_{20}$-structure factor is ascribed to the partial $S_{BB}(Q)$ with the assumption that the main maximum of $S_{BB}(Q)$ should be symmetrical with a height of three. In Fig. 4 the additional peak at $Q \cong 21.5\,nm^{-1}$ is presented. In addition to the S_{tot}^{57}-scale at the left hand side Fig. 4 also shows an S_{BB}-scale at the right hand side (rhs).

The relationship between the two scales is given as follows: From (1) we obtain with the W_{ij} from Table 3:

$$\begin{aligned} S_{tot}^{57} &= 0.0713\,S_{BB} \\ &\quad + (0.5374\,S_{FeFe} + 0.3913\,S_{FeB}) \\ &= 0.0713\,S_{BB} + D\,. \end{aligned}$$

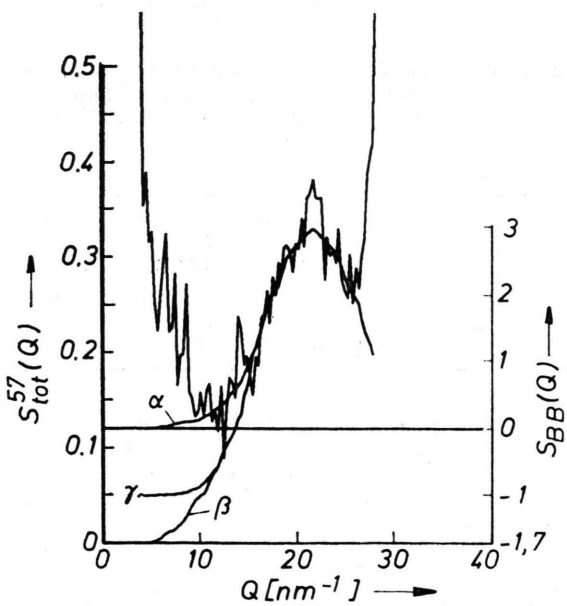

Fig. 4. Total structure factor $S_{tot}^{57}(Q)$ for small Q's with possible extrapolation of possible $S_{BB}(Q)$-Factors. The two ordinates are connected by $S_{tot}^{57}(Q) + 0.12 = 0.0713\,S_{BB}(Q)$.

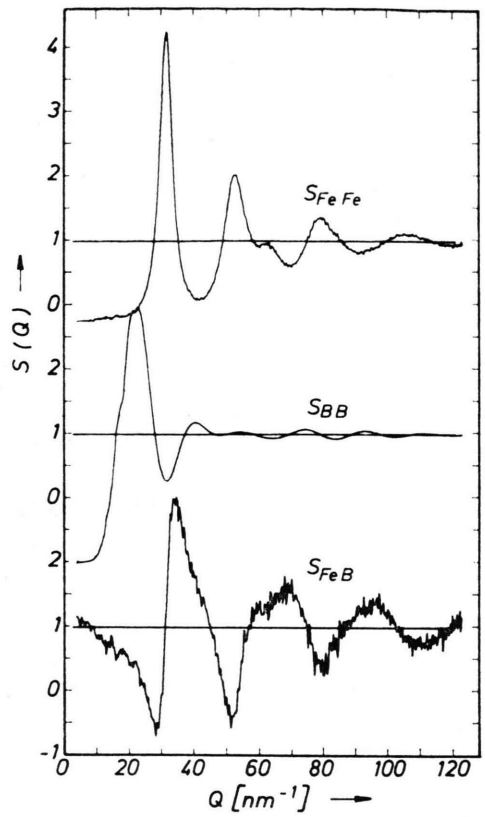

Fig. 5. Amorphous $Fe_{80}B_{20}$: Partial FZ-Structure factors.

From this equation follows at $Q = 21.5\,nm^{-1}$ with $S_{tot}^{57} = 0.33$ and with $S_{BB} = 3$; $D = 0.12$, which corresponds according to Fig. 4 to $S_{BB} = 0$ at the rhs.

For small Q-values the $S_{BB}(Q)$-curve was extrapolated using the run β of Fig. 4 which fulfills the inequations given in [20] and which yields a shape of the S_{BB}-maximum which is reasonable compared to results of the model calculations given in [19].

The final S_{BB}^{fit} structure factor was composed of this run for $Q < 15\,nm^{-1}$ and of three $(\sin Qr_i/Qr_i)$-curves attenuated exponentially for $Q > 15\,nm^{-1}$, were the three r_i were chosen in such a way that the resulting curve fits the experimental run of the peak in Figure 4. Fig. 5 shows this partial structure factor together with the two other FZ-partial structure factors calculated according to (14). The width of the main maximum of $S_{BB}(Q)$ is well described, and for $Q > 40\,nm^{-1}$ there is a mutual extinction of the oscillations. The S_{BB}^{fit}-structure factor from Fig. 5 shows a deviation $\Delta'(Q)$ compared to the $S_{BB}^{exp}(Q)$-structure factor obtained according to (14):

$$\begin{aligned} \Delta'(Q) &= S_{BB}^{exp}(Q) - S_{BB}^{fit}(Q) \\ &= (V_{21}(Q)\, S_{tot}^{X}(Q) + V_{22}(Q)\, S_{tot}^{nat}(Q) \\ &\quad + V_{23}(Q)\, S_{tot}^{57}(Q)) - S_{BB}^{fit}(Q). \quad (22) \end{aligned}$$

Assuming for each experiment the same error probability, to all $S_{tot}(Q)$ the same error $\Delta(Q)$ was ascribed:

$$\Delta(Q) = \Delta'(Q)/(\Sigma_j |\, V_{2j}(Q)\,|). \quad (23)$$

Figures 6a and 6b show the run of $\Delta(Q)$ and of its Fourier-transform. According to these curves the error is very small compared to the amplitudes of the curves in Figs. 2 and 3.

As expected from the weighting factors in Table 3 the $S_{FeFe}(Q)$ partial structure factor in Fig. 5 is very similar to $S_{tot}^{X}(Q)$.

$S_{FeB}(Q)$ exhibits pronounced maxima and minima. The main maximum is rather unsymmetrical. $S_{FeB}(Q)$ is very similar to $S_{AB}(Q)$ predicted by Blétry [19] for melts with short range order.

Figure 7 shows the partial BT-structure factors calculated from the partial FZ-structure factors of Figure 5. $S_{NN}(Q)$ is characterized by a pronounced main maximum and a shoulder at the right hand side of the second maximum. The further maxima and minima apparently are attenuated by an antiphase contribution in a similar way as $S_{tot}^{57}(Q)$.

The structure factor $S'_{CC}(Q)$ shows oscillations. This means that the atoms of both components are arranged in a non statistical way. The steep unsymmetrical decrease at the right hand side of the first maximum lies in the same Q-region as the unsymmetrical increase to the first maximum of the partial structure factor $S_{FeB}(Q)$ in Figure 5. $S'_{CC}(Q)$ shows an antiphase behaviour to $S_{FeB}(Q)$.

The structure factor $S_{NC}(Q)$ is similar to $S'_{CC}(Q)$ but more strongly attenuated in the region $Q \geqq 50\ nm^{-1}$. This means that the concentration fluctuations are correlated with density fluctuations. This fact results from the very different atomic diameters of Fe and B.

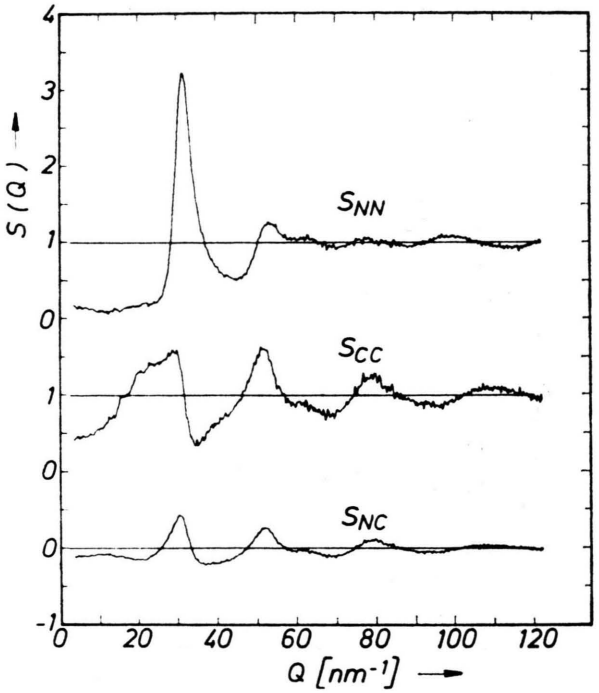

Fig. 7. Amorphous $Fe_{80}B_{20}$: Partial BT-Structure factors.

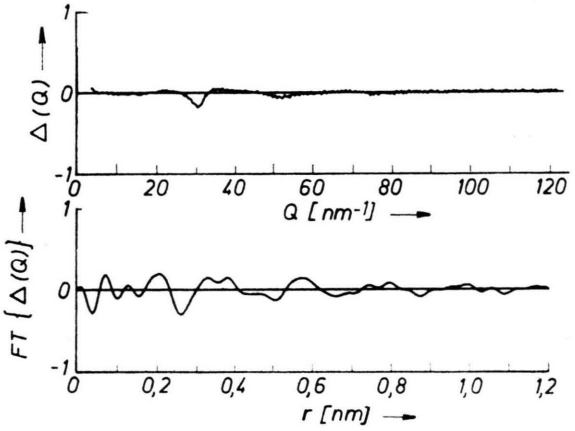

Fig. 6. Error $\Delta(Q)$ according to Eq. (23) and its Fourier-transform FT $\{\Delta(Q)\}$.

iii) *Partial Functions* $G_{ij}(r)$

Figure 8 shows the partial FZ-functions $G_{ij}(r)$. Table 7 contains the characteristic data taken from these curves.

$G_{FeFe}(r)$ is very similar to the total $G(r)$ from the X-ray experiment, the extrema, however, being more pronounced, as can be seen from the splitting up of the second maximum. The second maximum is separated very distinctly from the third maximum thus indicating well defined coordination shells.

The Fe-B correlation function $G_{FeB}(r)$ shows very interesting features: The extremely sharp and pronounced first maximum reflects a very well defined Fe-B distance. Concerning the half maximum full width of this peak ($\delta r^{exp} = 0.05$ nm) it

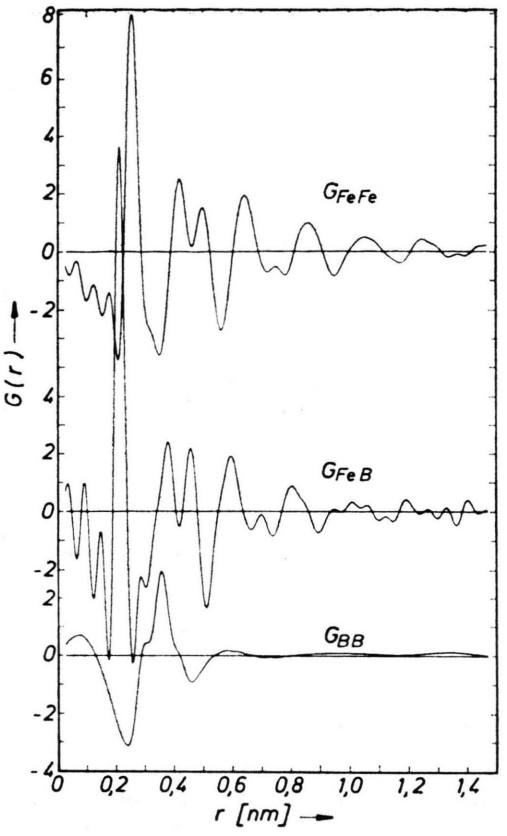

Fig. 8. Amorphous $Fe_{80}B_{20}$: Partial reduced FZ-pair distribution functions $G_{ij}^{FZ}(r)$.

should be noted that it results from the real width of the Fe-B distance distribution of the amorphous structure ($\delta r^{str.}$) by broadening due to the finite Fourier transformation in Q-space. Assuming a Gaussian distribution, the effect of broadening can be calculated thus yielding for the real width $\delta r^{str.} = 0.02$ nm, which is very small. From this very well defined Fe-B atomic distance we must conclude that the short range order in metallic glasses of the $T_{80}M_{20}$-type is governed strongly by chemical bonding between unlike atoms. This means that the small boron atoms force a special arrangement of the Fe atoms by chemical interaction rather than by just filling up the free space in a Bernal like dense random packing of the Fe atoms as proposed by Polk [21]. From $G_{BB}(r)$ the B-B-distance was evaluated to be $r_{BB} \cong 0.355$ nm.

Figure 9 shows the Fourier-transformations of the partial BT-structure factors. $G_{NN}(r)$ represents the correlation of density fluctuations. The short B-Fe distance is indicated as a shoulder at the left hand side of the first maximum. The second maximum is rather unsymmetrical with a shoulder at the rhs. The further maxima show no pronounced details and have a mutual distance of 0.21 nm. The run of $G_{NN}(r)$ shows that the atoms are fixed in distinct coordination spheres up to rather large distances.

Table 7. Height and position of maxima and minima of the partial $S_{ij}(Q)$ and the partial $G_{ij}(r)$. $[Q] = \text{nm}^{-1}$; $[r] = \text{nm}$.

ij	$S_{ij}(Q)$ $Q \cong 4\ \text{nm}^{-1}$	$S_{ij}^{I}(Q)$ (Q^{I})	$G_{ij}^{I}(r)$ (r^{I})	$G_{ij}^{II,1}(r)$ $(r_{ij}^{II,1})$	$G_{ij}^{II,2}(r)$ $(r_{ij}^{II,2})$	$G_{ij}^{III}(r)$ (r_{ij}^{III})	$G_{ij}^{IV}(r)$ (r_{ij}^{IV})
FeFe	− 0.24	4.2 (31.1)	8.51 (0.257)	2.51 (0.420)	1.54 (0.498)	2.0 (0.645)	1.0 (0.86)
BB	(− 1)	3.0 (21.5)	2.9 (0.357)				
FeB	≅ 1	3.0 (33.0)	12.63 (0.214)	2.41 (0.379)	2.20 (0.457)	1.92 (0.595)	0.87 (0.805)
NN	0.15	3.2 (31.3)	3.75 (0.257)	1.53 (0.420)	0.81 (≅ 0.46)	1.28 (0.63)	0.72 (0.845)
CC	0.4	1.6 (30.0)	2.7 (0.258)	0.6 (0.418)	1.2 (0.510)		
			− 5.0 (0.214)	− 0.77 (0.378)	− 0.82 (0.457)		
NC	− 0.1	1.4 (30.4)	1.7 (0.257)	0.39 (0.419)	0.50 (0.505)		
			− 1.6 (0.213)	− 0.63 (0.360)	− 0.15 (0.458)		

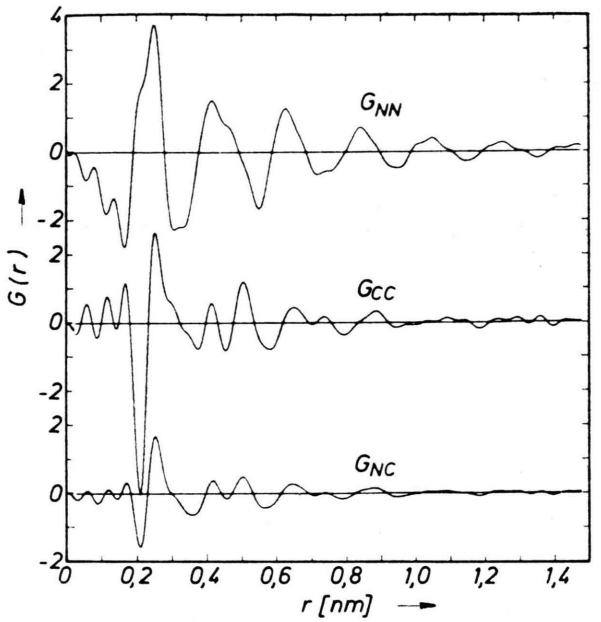

Fig. 9. Amorphous $Fe_{80}B_{20}$: Fourier-transforms of the partial $S_{ij}^{BT}(Q)$-Structure factors.

The partial function $G_{CC}(r)$ represents the correlation of concentration fluctuations. This function is plotted in Fig. 10 together with $G_{FeFe}(r)$ and $G_{FeB}(r)$. The maxima of $G_{FeB}(r)$ coincide with the minima of $G_{CC}(r)$ and the maxima of $G_{FeFe}(r)$ have nearly the same positions as the maxima of the $G_{CC}(r)$-curve. This means that the experimental $G_{CC}(r)$ fullfills the theoretical requirement being >0 for like neighbours and <0 for unlike neighbours. The run of the $G_{NC}(r)$ curve in Fig. 9 indicates a considerable cross correlation of density- and concentration fluctuations as expected from the very different atomic diameters of Fe and B.

In Fig. 11 the partial function G_{FeB} from Fig. 8 is shifted in such a way that the first maxima of the G_{FeFe}- and G_{FeB}-curve lie at the same r-position. Interestingly by this shift the positions of the second, third etc. maximum of the two curves coincide, whereby the oscillations of the G_{FeB}-curve are more pronounced. This coincidence of the maxima will play a deciding role during the construction of models for the description of the atomic arrangement in the metallic T-M-type glasses.

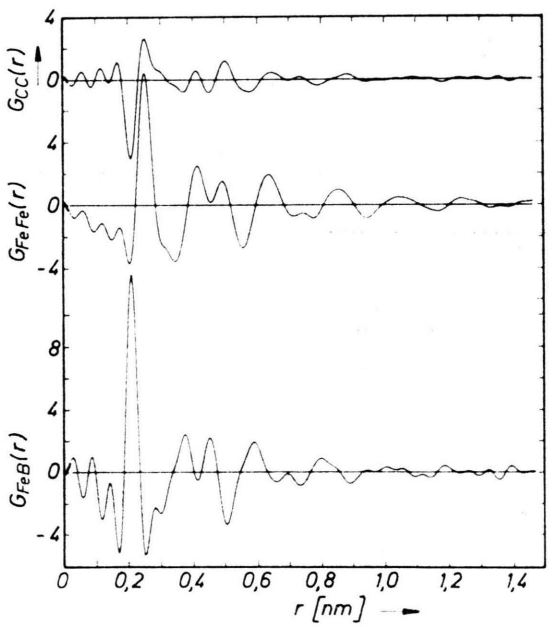

Fig. 10. Amorphous $Fe_{80}B_{20}$: Fourier-transforms $G_{FeFe}(r)$, $G_{FeB}(r)$ and $G_{CC}(r)$ of the corresponding partial structure factors.

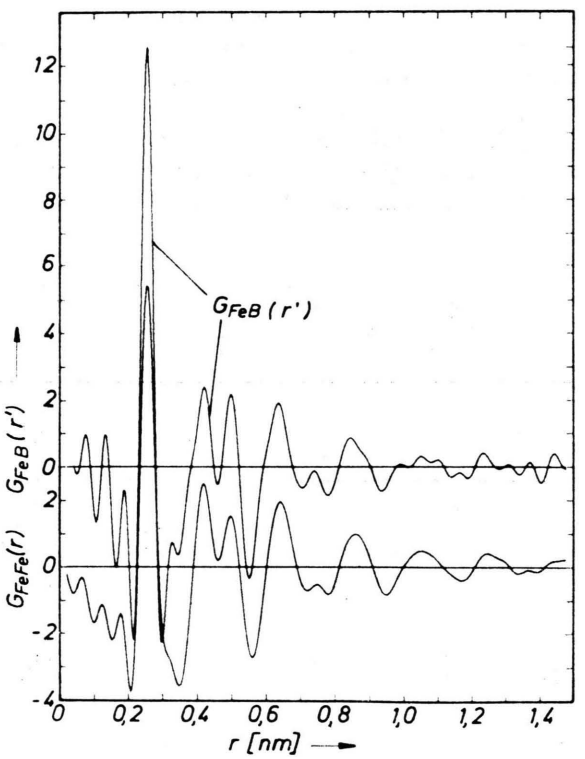

Fig. 11. Amorphous $Fe_{80}B_{20}$: Partial Functions $G_{FeFe}(r)$ and $G_{FeB}(r')$, wobei

$$r' = r - (r^{I}_{FeFe} - r^{I}_{FeB}).$$

iv) *Partial Distances and Coordination Numbers*

From the position of the maxima in the partial reduced pair distribution functions $G_{ij}(r)$ the preferred distances between the different atoms can be determined. According to Table 7 neighbouring Fe-Fe atoms have a distance of 0.257 nm. This value is in good accordance with the Goldschmidt-diameter of iron for coordination number twelve (0.254 nm according to [22]).

According to Table 7 neighbouring Fe-B atoms show a distance of 0.214 nm. Presuming the iron diameter to be independent of the kind of the neighbours the radius of the Boron atom can be calculated according to (24):

$$r_B = r^I_{FeB} - 0.5\, r^I_{FeFe}. \tag{24}$$

The value of 0.086 nm thus obtained is in good accordance with 0.083 nm given in [23] as radius of a covalently bound Boron atom in tetrahedrical surrounding with four nearest neighbours.

From the partial $G_{ij}(r)$-curves the partial coordination numbers can be obtained. To calculate the coordination numbers given in Table 8 the integration always was performed from the lower minimum r_l up to the upper minimum r_u in the $A_{ij}(r)$-curves. The coordination numbers $Z^{n,m}_{ij}$ of the m-th submaximum within the n-th coordination sphere are given. From these figures the total coordination numbers $N^{n,m}_c$ can be calculated according to (16) using the weighting factors of Table 3, and finally the $N^{n,m}_c$ can be compared to the $N^{n,m}_{exp}$ of Table 2.

v) *Long Wavelength Limit of $S'_{CC}(Q)$*

In the long wavelength limit, i.e. for $Q=0$ the following relation holds for melts in thermodynamic equilibrium:

$$\frac{RT}{c_{Fe}\, c_B\, S'_{CC}(0)} = \frac{RT}{N\langle \Delta c^2\rangle} = \frac{\partial^2 G}{\partial c^2} = E^{XS} + \frac{RT}{c_{Fe}\, c_B} \tag{25}$$

with $\langle \Delta c^2\rangle$ mean quadratic concentration fluctuation; G free enthalpy, $E^{XS} = -RT\,\partial \ln \gamma_{Fe}/\partial c^2{}_B =$ Darken's excess stability function, γ_{Fe} activity coefficient of iron.

Since amorphous alloys are nonequilibrium systems, the relationship (25) between $S'_{CC}(o)$ and thermodynamic data is not applicable. Assuming the amorphous substance to represent a frozen undercooled melt at the glassforming temperature T_g and furthermore that this state is not yet changed by relaxation phenomena, the following estimation can be done:

$$E^{XS} = 9.38\, RT = 54.6\ \text{kJ/mol}$$

using $S'_{CC}(o) \cong 0.4$ and $T_g \cong 700$ K (see [24]).

Table 8. Partial coordination numbers $Z^{n,m}_{ij}$. $Z^{n,m}_{ij}$: number of j-atoms within the m-th maximum of the n-th coordination sphere around an i-atom. $Z^{n,m}_{NN}$: number of atoms around an averaged central atom (example: $Z^I_{NN} = c_{Fe}(Z^I_{FeFe} + Z^I_{FeB}) + c_B(Z^I_{BFe} + Z^I_{BB})$). $Q_{max}[nm^{-1}]$: upper integration limit for the Fourier-transform. r_l, r_u[nm]: lower, upper integration limit during the calculation of partial coordination numbers.

ij (Q_{Max})	Z^I_{ij} $\binom{r_l}{r_u}$	$Z^{II,1}_{ij}$ $\binom{r_l}{r_u}$	$Z^{II,2}_{ij}$ $\binom{r_l}{r_u}$	Z^{III}_{ij} $\binom{r_l}{r_u}$	$Z^{III,A}_{ij}$ $\binom{r_l}{r_u}$	Z^{IV}_{ij} $\binom{r_l}{r_u}$
FeFe (113)	12.4 (0.225 / 0.345)	18.1 (0.350 / 0.460)	24.6 (0.465 / 0.560)	58 (0.565 / 0.705)	—	144 (0.710 / 0.930)
BB (122)		6.5 (0.250 / 0.445)	—	—	—	—
BFe (118)	8.64 (0.190 / 0.255)	15.2 (0.305 / 0.415)	19.3 (0.420 / 0.510)	46.4 (0.515 / 0.650)	32 (0.655 / 0.720)	97 (0.730 / 0.880)
FeB	2.16	3.8	4.8	11.6	4	24
NN (122)	12.7 (0.185 / 0.310)	20.6 (0.315 / 0.440)	31.9 (0.445 / 0.550)	75 (0.555 / 0.705)	—	—

In [25] for an amorphous $Ti_{40}Ni_{60}$-alloy also from $S_{CC}(o)$ a value of 60 kJ/mol was obtained, which also was calculated under the presumptions explained above.

vi) *Short Range Order Parameter*

In amorphous $Fe_{80}B_{20}$ the atoms of both kinds exhibit very different atomic diameters and therefore cannot be substituted. Therefore Cowley's short range order parameter [26] is not applicable for amorphous $Fe_{80}B_{20}$, and we will be concerned in the following with the short range order parameter according to Cargill and Spaepen [27]. This kind of short range order parameter was introduced for the cases where the A atoms show a coordination number Z_A different from the coordination number Z_B of the B-atoms.

For a statistical distribution of the atoms the entropy of the atomic distribution shows a maximum. The deviation from this arrangement with maximum entropy is connected with a short range order parameter η_{AB}. η_{AB} is zero for a statistical distribution, >0 for a compound forming tendency and <0 for a segregation tendency. The short range order parameter for amorphous $Fe_{80}B_{20}$ can be calculated as follows:

$$\eta^{I}_{FeB} = Z_{FeB}/Z^{*}_{FeB} - 1 \qquad (26)$$

with $Z^{*}_{FeB} = c_B Z_B Z_{Fe}/(c_{Fe}Z_{Fe} + c_B Z_B)$ = number of B-atoms around an Fe-atom for statistical distribution of the atoms. With the figures from Table 8 we obtain $Z^{*}_{FeB} = 1.88$ and $Z_{FeB} = 2.16$ which yields

$$\eta^{I}_{FeB} = 0.148\,.$$

This means a preferred compound forming tendency in amorphous $Fe_{80}B_{20}$. A normalized short range order parameter $\eta^{I,o}_{FeB}$ is obtained if we normalize η^{I}_{FeB} to the maximum possible value $\eta^{I,max}_{FeB} = c_B Z_B/c_{Fe}Z_{Fe}$:

$$\eta^{I,o}_{FeB} = 1.0\,.$$

This means maximum chemical short range order in amorphous $Fe_{80}B_{20}$. It should be mentioned that according to [27] also amorphous $Co_{80}P_{20}$ and $Pd_{80}Si_{20}$ exhibit normalized short range order parameters equal to unity.

vii) *Description of the Short Range Order of the Amorphous Alloy $Fe_{80}B_{20}$*

Amorphous $Fe_{80}B_{20}$ crystallizes to metastable Fe_3B with the averaged coordination numbers $Z_{BFe} = 9$; $Z_{FeB} = 3$; and $Z_{FeFe} = 10.7$. The comparison with the corresponding figures 8.64; 2.16; and 12.4 for the amorphous alloy $Fe_{80}B_{20}$ in Table 9 shows good agreement for Z_{BFe} within the experimental errors. From this agreement, and especially regarding the very pronounced narrow main maximum in the G_{FeB}-curve of Fig. 8, the following model for amorphous $Fe_{80}B_{20}$ can be proposed. The B-atoms can be regarded as the centre of a coordination sphere containing nine iron atoms. Within such a region with its pronounced short range order an atomic arrangement exists which is comparable to that of metastable Fe_3B. This boron coordination is assumed not to change with concentration, which is supported by the same observation made during the computer calculations in [28, 29]. Taking into account the fact that the amorphous alloy $Fe_{80}B_{20}$ contains 5 a/o more Fe than crystalline Fe_3B, one can explain that Z_{FeFe} is higher and Z_{FeB} is smaller than the corresponding value in the crystalline Fe_3B-state.

Figure 12 shows an atomic arrangement where the diameter of the Fe atom is 0.254 nm [22] and that of the B atom is 0.176 nm [23]. This yields a B-B distance of 0.347 nm which is in good agreement with the experimental value $r^{I}_{BB} = 0.357$ of the present study.

viii) *Comparison with Existing Models*

There is a lot of attempts to model the structure of T-M-glasses. Any model which describes this structure should take into consideration at least two requirements: The different size of the two kinds of atoms and the strong interaction between the metal and metalloid atoms compared to that between the metal atoms.

Sadoc et al. [30] have constructed a computer generated DRPHS-model of spheres with different sizes. Preferred interaction between large and small spheres was simulated by excluding direct contact between the small spheres. One of the results was that small spheres are always surrounded by 9 large

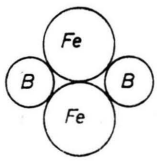

Fig. 12. Amorphous $Fe_{80}B_{20}$: Arrangement of nearest iron- and boron-neighbours.

spheres, which is in accordance with the present work. However, when applying the model to $Ni_{84}P_{16}$ they obtained a partial $G_{NiP}(r)$-function the width of their first peak being much broader than the width of the present $G_{FeB}(r)$-curve. This indicates that the simulation of the chemical interaction should be even stricter in a more realistic model.

Boudreaux et al. [28, 29] have energetically relaxed a hard sphere structure with two atomic diameters using modified Lennard-Jones potentials to construct a model for amorphous Fe-B-alloys. The chemical interaction was simulated by chosing the metal-metalloid interaction to be twice as strong as that between the metal atoms, and that between metalloid atoms to be very weak. They found each Boron-atom to be surrounded by 6.6 Fe atoms, which is considerably less than the value of 8.6 atoms derived experimentally in the present study. Furthermore the splitting up of the second maximum of $S(Q)$ of the model is not as pronounced as with the present experiment. In a recent paper, Fujiwara et al. [31] modelled the structure of amorphous $F_{83}B_{17}$ by relaxing a DRP structure with truncated Morse-type potentials. They compared the results with experimental $G_{FeFe}(r)$- and $G_{FeB}(r)$-functions. The latter have been estimated by combining a neutron- and an X-ray diffraction experiment. The experimental $G_{FeB}(r)$ shows considerable differences to the corresponding one of the present work (no splitting up of the second maximum, $r_{FeB} = 0.227$ nm, $Z_{BFe} = 6.9$) as well as to the $G_{FeB}(r)$ curve of the model. However, comparing the model curves in [31] with the partial $G_{ij}(r)$-curves of this study one finds quite good agreement: The first peak of $G_{FeB}(r)$ is more pronounced than that of $G_{FeFe}(r)$. The second subpeak of the splitted second maximum of G_{FeB} coincides with the minimum between the two subpeaks of the second maximum of G_{FeFe}. The maximum of G_{BB} at $\cong 0.38$ nm falls into the range of the first subpeak of the second maximum of $G_{FeB}(r)$. But there are also differences, and one should keep in mind the slightly different composition of the model system and the specimen investigated in the present work.

Acknowledgements

Thanks are due to the Deutsche Forschungsgemeinschaft, Bad Godesberg, for the financial support of this work and to the Laue Langevin Institute, Grenoble, for granting measuring time at different instruments around the high flux reactor.

[1] R. W. James, The Optical Principles of the Diffraction of X-rays, G. Bell and Sons LTD, London 1958.
[2] V. F. Turchin, Slow Neutrons, Sivan Press, Jerusalem 1965.
[3] C. N. J. Wagner, J. Non-Cryst. Solids **31**, 1 (1978).
[4] G. S. Cargill III, Sol. Stat. Phys. **30**, 227 (1975).
[5] T. E. Faber and J. M. Ziman, Phil. Mag. **11**, 153 (1965).
[6] A. Boos, P. Lamparter, and S. Steeb, Z. Naturforsch. **32a**, 1222 (1977).
[7] N. W. Ashcroft and D. C. Langreth, Phys. Rev. **156**, 685 (1967).
[8] G. E. Bacon, Neutron Diffraction, third edition, Clarendon Press, Oxford 1975.
[9] P. Lamparter, W. Knoll, and S. Steeb, Z. Naturforsch. **31a**, 90 (1976).
[10] A. B. Bhatia and D. E. Thornton, Phys. Rev. **B2**, 3004 (1970).
[11] W. Sperl, Diplom-Thesis, University of Stuttgart 1980.
[12] Neutron Beam Facilities at the HFR available for Users, ILL, Grenoble 1977.
[13] G. Rainer-Harbach, Doctor-Thesis, University of Stuttgart 1979.
[14] J.-P. Gabathuler, Doctor-Thesis, University of Stuttgart 1978.
[15] Y. Waseda and H. S. Chen, Phys. Status Solidi (a) **49**, 387 (1978).
[16] S. Steeb and M. Weber, Gießereiforschung **31**, 101 (1979).
[17] P. Lamparter, E. Nold, G. Rainer-Harbach, E. Grallath, and S. Steeb, Z. Naturforsch. **36a**, 165 (1981).
[18] P. F. J. Poncet, Doctor-Thesis, University of Reading, Reading 1976.
[19] J. Blétry, Z. Naturforsch. **33a**, 327 (1978).
[20] J. E. Enderby, D. E. North, and P. A. Egelstaff, Phil. Mag. **14**, 961 (1966).
[21] D. E. Polk, Acta Met. **20**, 485 (1972).
[22] W. Hume Rothery and G. V. Raynor, The Structure of Metals and Alloys, 3rd ed., Inst. Metals London 1954, p. 94.
[23] L. Pauling, The Nature of the Chemical Bond, 3rd. ed., Ithaca, Cornell Univ. Press New York 1960, p. 246.
[24] H. A. Davies, Rapidly Quenched Metals III, Brighton (1) 1978, p. 1.
[25] H. Ruppersberg, D. Lee, and C. N. J. Wagner, J. Phys. F: Metal Phys. **10**, 1645 (1980).
[26] J. M. Cowley, J. Appl. Phys. **21**, 24 (1950).
[27] G. S. Cargill III and F. Spaepen, J. Non-Cryst. Solids **43**, 91 (1981).
[28] D. S. Boudreaux, Phys. Rev. **B18**, 4039 (1978).
[29] D. S. Boudreaux and J. M. Gregor, J. Appl. Phys. **48**, 5057 (1977).
[30] J. F. Sadoc, J. Dixmier, and A. Guinier, J. Non-Cryst. Solids **12**, 46 (1973).
[31] T. Fujiwara, H. S. Chen, and Y. Waseda, J. Phys. F: Metal Phys. **11**, 1327 (1981).